

Integration of bulk materials with two-dimensional materials for physical coupling and applications

Sang-Hoon Bae^{1,2}, Hyun Kum^{1,2}, Wei Kong^{1,2}, Yunjo Kim^{1,2}, Chanyeol Choi^{2,3}, Byunghun Lee^{1,2}, Peng Lin^{1,2}, Yongmo Park^{1,2} and Jeehwan Kim^{1,2,4*}

Hybrid heterostructures are essential for functional device systems. The advent of 2D materials has broadened the material set beyond conventional 3D material-based heterostructures. It has triggered the fundamental investigation and use in applications of new coupling phenomena between 3D bulk materials and 2D atomic layers that have unique van der Waals features. Here we review the state-of-the-art fabrication of 2D and 3D heterostructures, present a critical survey of unique phenomena arising from forming 3D/2D interfaces, and introduce their applications. We also discuss potential directions for research based on these new coupled architectures.

Heterostructures composed of two-dimensional (2D) layered materials and three-dimensional (3D) bulk materials that have dangling bonds at their surface have generated great interest because of the unique functionalities arising from this integration¹. Interfacing 3D and 2D materials, with band alignment strongly influenced by the unique nature of each material system, enables drastic changes in the electrical, magnetic, optical and thermal properties beyond those of the individual materials^{2–6}. Thus, appropriate selection of 3D and 2D materials can allow significant modification of their physical structures, resulting in intriguing properties and unprecedented device architectures. While constructing 2D materials on 3D materials (2D-on-3D) heterostructures is well established by transfer or van der Waals epitaxy (vdWE) techniques, recent progress made on growing single-crystalline 3D materials on 2D materials (3D-on-2D) can offer great flexibility for the design of mixed heterostructures and push forward the use of 2D materials in a large range of industrial applications.

In this Review, we summarize 2D-on-3D and 3D-on-2D integration methods, with particular focus on the advanced growth techniques to achieve high-quality 3D crystals on 2D materials. For clarity, when our considerations do not specifically depend on the assembly order of the heterostructure, we will refer more generally to 3D/2D systems or interfaces. Following suit, we present 3D/2D physical coupling phenomena and their applications in various fields, which can bring extensive functionality to conventional 3D materials-based device structures. The integration of 2D and 3D materials may help implement 2D materials in industrially viable technologies.

Fabrication of 3D/2D heterostructures

Although well-established 2D material transfer or vdWE (epitaxial growth that proceeds on a vdW surface) processes have facilitated the fabrication and study of 2D-on-3D heterostructures in recent years, the realization of 3D-on-2D heterostructures is still at a premature stage. Reports on vdWE^{7,8} have also inspired the synthesis of strain-relaxed, epitaxial 3D materials on 2D materials with substantially high lattice mismatch. Still, growing planar single-crystalline films of 3D materials remains challenging due to the poor wettability of the vdW surface of layered materials and suppressed nucleation thereof. This section starts with a survey on the methods to form 2D-on-3D heterostructures followed by the mechanisms to grow high-quality 3D crystals on layered materials (Fig. 1a).

2D-on-3D fabrication. 2D-on-3D heterostructures have been fabricated either by transferring or growing 2D materials on 3D materials, in particular with vdWE techniques that secure pristine interfaces of 2D-on-3D heterostructures, while substantially relaxing lattice-matching rules. The discovery of vdWE came in the mid-1980s during the epitaxial growth of Se on Te^{7,8}. In a conventional epitaxy process, dangling bonds are present at the substrate surface, leading to chemical bonding of adsorbates. In a vdWE process, adsorbates bind to the substrate surface by vdW forces, without transferring or sharing of electrons. This enables the formation of heterostructures with large lattice mismatch, resulting in highly textured polycrystalline 2D materials on the substrates because of high strain energy. Although the synthesis of single-crystalline, defect-free films is generally desirable to better exploit the intrinsic electronic properties of a material, it has been reported that the presence of grain boundaries in 2D materials is less detrimental to the device performance with respect to polycrystalline 3D materials^{9,10}. However, film thickness is a more critical parameter for 2D materials because their physical properties can drastically change with the number of layers^{11,12}. Precise thickness control is in general still extremely challenging. Examples have been reported where management of nucleation and coalescence of monolayer 2D materials on 3D substrates has allowed the synthesis of transition metal dichalcogenides (TMDs) with controlled number of layers¹³. Compared to other 2D materials, growth of monolayer graphene has been well established. For instance, monolayer epitaxial graphene can be obtained by sublimating Si atoms from SiC wafers through self-limiting graphitization process, or by growing monolayer graphene on (011) Ge wafers^{14,15}.

While vdWE ensures the formation of pristine 2D-on-3D interfaces, many factors such as the type of substrate, precursors, temperature and pressure must be precisely designed to obtain high-quality heterostructures. Transfer of 2D materials is not affected by these constraints, thus it can be more flexible for the design of 2D-on-3D heterostructures; however, the interfaces can be contaminated during the transfer process. Early investigations used mechanical transfer of 2D flakes onto 3D substrates by the scotch tape method¹⁶. While this has been useful to prove the concept of heterostructures, this method cannot be used for large-scale manufacturing due to limited reproducibility and the limited size of transferred 2D materials. Later, a more controllable and scalable process was developed

¹Mechanical Engineering, Massachusetts Institute of Technology, Cambridge, MA, USA. ²Research Laboratory of Electronics, Massachusetts Institute of Technology, Cambridge, MA, USA. ³Department of Electrical Engineering and Computer Science, Massachusetts Institute of Technology, Cambridge, MA, USA. ⁴Materials Science and Engineering, Massachusetts Institute of Technology, Cambridge, MA, USA. *e-mail: jeehwan@mit.edu

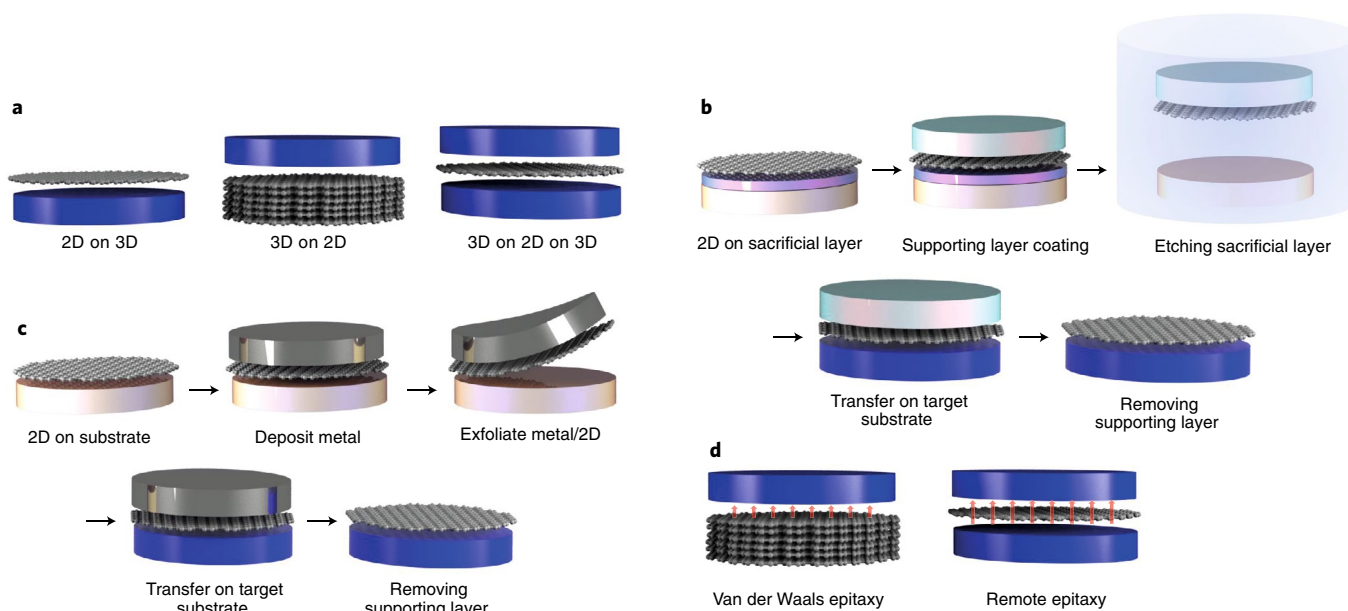


Fig. 1 | 3D/2D structures and fabrication methods. **a**, Schematics of coupling structures. **b**, Schematics of representative wet transfer of 2D materials using a supporting layer. **c**, Schematics of representative quasi-dry transfer of 2D materials using a metal supporting layer. **d**, Schematics of vdWE and remote epitaxy.

by wet transfer of grown 2D materials^{17–20} (Fig. 1b). In such case, thin 2D materials coated with polymer handlers are dipped into wet chemical etching solutions to separate them from the catalyst substrates. The freestanding polymer/2D material stack is subsequently scooped by the target 3D substrate from the solution and eventually the polymer handler is chemically dissolved. While the process can be scaled up to stack complex heterostructures, the quality of 2D/3D interfaces deteriorates due to the direct contact of the 2D material surface with the wet chemical solution²¹. Further improvements have been made by adopting a metal-induced quasi-dry transfer process, where 2D materials are peeled off from the growth substrates using a metal handler in dry environment, and immediately bonded to the surface of the target 3D substrates^{22–25} (Fig. 1c). As such, metal-induced transfer can ensure the formation of clean 2D-on-3D interfaces. While the most attractive aspect of these transfer techniques is their applicability to a wide range of materials without thermal and chemical limitations, process residues such as polymers or metals are unavoidable on the surface of 2D materials.

3D-on-2D fabrication. To form high-performance 3D-on-2D heterostructures, it is essential to grow high-quality single-crystalline 3D materials on 2D materials (Fig. 1d). Recently, attempts to use vdWE to grow bulk thin film materials on vdW surfaces have been reported^{26–32}. However, several challenges remain before vdWE can become the mainstream epitaxial process for 3D-on-2D systems. First, although vdWE greatly relaxes the requirement of lattice matching, the weak interaction between substrate and epilayer can cause incommensurate short-range ordering in the epilayer. Current studies show that 3D overlayers can nucleate on layered materials substrates, but with only partial epilayer–substrate epitaxial alignment across the epitaxial films. This leads to a polycrystalline epilayer with a textured grain structure. For example, GaAs growth on graphene typically results in forming highly oriented polycrystalline GaAs films owing to graphene’s weak interactivity³³ (see Fig. 2a). Second, vdWE of 3D overlayers on 2D substrates tends to form rough surfaces^{29,30} (see Fig. 2b). Due to the absence of reactive dangling bonds at the epitaxial surface, the wettability of 2D substrate is relatively poor, leading to the Volmer–Weber growth mode and a

tendency of cluster formation. In extreme cases, vertical nanowire structures can be formed during direct growth of various semiconductor materials on 2D substrates^{28,34,35}.

Considerations must be made to enhance the wettability and interactivity on 2D substrate to mitigate these effects. For example, a ZnO nanowall buffer layer was deposited prior the GaN growth on graphene, achieving a reasonably smooth surface²⁶ (Fig. 2c). However, a porous ZnO buffer layer led to in-plane rotation of the GaN grains (Fig. 2d)³⁶. More recently, by using a hexagonal boron nitride (hBN) substrate together with a highly sticking buffer layer such as AlGaIn, a perfect single-crystalline GaN with atomically smooth surface (Fig. 2e,f) was demonstrated^{27,31}. In this case, two crucial conditions are satisfied as the AlGaIn buffer enhances wettability and hBN interacts strongly with AlGaIn. So far, only hBN substrates demonstrated the ability to seed the growth of planar 3D III–N single-crystalline films^{27,31}; material systems that can be grown by vdWE as planar single crystals have been very limited. Further innovations in the fundamental understanding and control of epitaxial growth on 2D material substrates are necessary to achieve high-quality 3D-on-2D heterostructures for arbitrary material systems.

We now focus in particular on the efforts to grow single-crystalline films on graphene. The majority of previous efforts have been made on epitaxy of 3D materials on polycrystalline graphene grown by chemical vapour deposition and transferred onto SiO₂/Si wafers. In most of these cases, however, the grown epitaxial layers (such as GaAs and GaN) show highly textured out-of-plane polycrystallinity^{29,33} in contrast with the case where thick hBN/sapphire substrates are used^{27,31}. This may be due to a reduced interactivity of graphene with adatoms compared to that of hBN. In another experiment, graphene transparency to chemical interaction has been proven by observing that the wetting angle of water droplets on graphene depends on the underlying substrate. Additional hints that substrate properties are able to penetrate one or few layers of graphene have been provided by the different growth modes of nanowires on various graphene-coated substrates³⁷. Thus, the substrate beneath graphene could play a role in determining the epitaxial orientation. Recently, the remote seeding effect from the substrate through

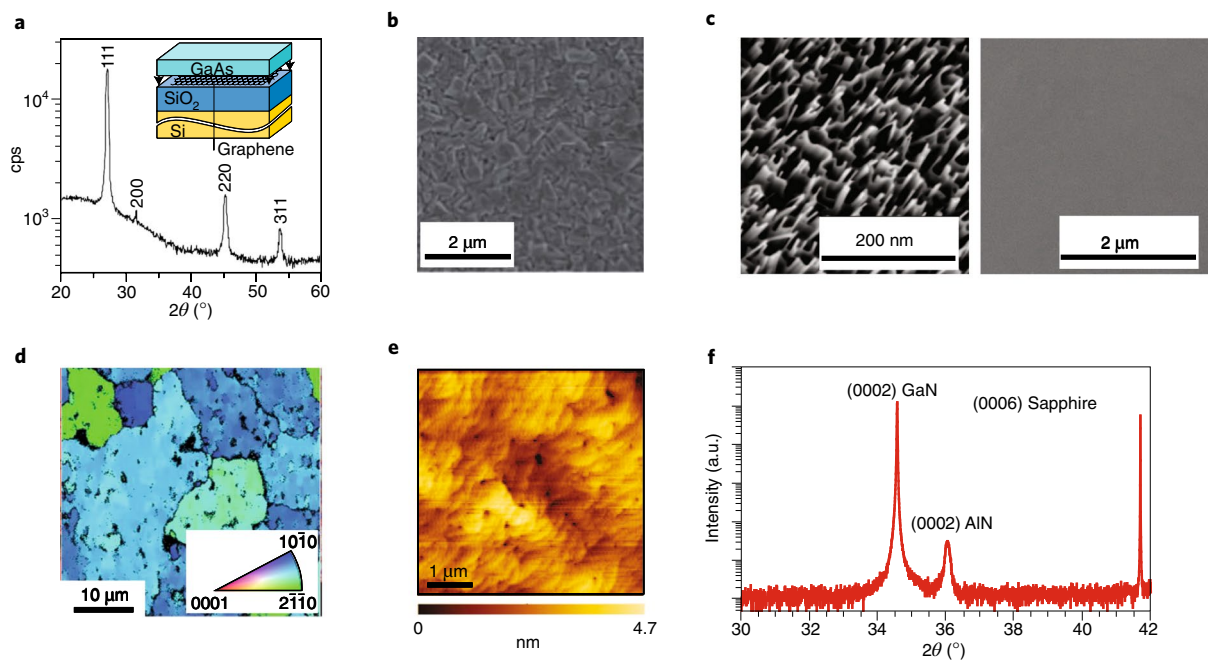


Fig. 2 | Van der Waals epitaxy of various materials on 2D materials. **a**, X-ray diffraction (XRD) spectra of highly textured, polycrystalline GaAs grown on graphene transferred on a SiO₂/Si substrate. **b**, Scanning electron microscopy (SEM) image of GaN grown on graphene transferred on a SiO₂/Si substrate. **c**, SEM images of ZnO nanowalls grown on graphene transferred on SiO₂/Si substrate (left) and GaN grown on ZnO nanowalls (right). **d**, Electron backscatter diffraction (EBSD) inverse pole figure maps in the transverse direction on GaN grown on ZnO nanowalls on graphene. **e**, Atomic force microscopy topology of GaN grown on thick single-crystalline hBN/sapphire substrate showing atomic smooth surface with root mean square roughness of 0.69 nm. **f**, High-resolution XRD spectra taken from GaN grown on thick single-crystalline hBN/sapphire substrate showing perfect single-crystallinity. Reproduced from ref. ³³, Elsevier (**a**); and ref. ²⁷, SNL (**e,f**). Adapted from ref. ²⁹, Elsevier (**b**); ref. ²⁶, AAAI (**c**); and ref. ³⁶, AIP (**d**).

graphene has been proven by growing wafer-scale (001) GaAs single-crystalline films on one monolayer (ML) graphene-coated (001) GaAs wafers²⁵. As shown in Fig. 3a, GaAs atoms in the films are aligned to those in the substrate, notwithstanding the gap created by 1 ML of graphene. This type of epitaxy is defined as remote epitaxy. Wafer-scale single-crystallinity is confirmed by electron backscatter diffraction (EBSD) mapping (Fig. 3a). This result also suggests that recent successful epitaxy of perfect single-crystalline GaN on 1 ML epitaxial graphene on 4H-SiC substrates can be attributed to remote epitaxy effects³⁸. Later, it was proven that remote epitaxy can be applied to grow perfect single-crystalline films of various ‘compound materials’ on graphene-coated wafers³⁹ (Fig. 3b). Direct epitaxial growth through defects in the graphene layer has been excluded by demonstrating that the grown epilayers can be peeled off and released without damage. While remote epitaxy occurs successfully for compound materials, attempting remote epitaxy of elemental semiconductors such as Si and Ge resulted in the formation of polycrystalline films³⁹. In fact, the majority of the area of Ge films grown on graphene/Ge wafers is polycrystalline, and substrate orientation is reflected in the epitaxial Ge films only when direct epitaxy through graphene defects or holes occurs. In this case, this shows insufficient potential field penetration from the elemental semiconductor substrate through graphene³⁹. Through further experiments and density functional theory calculations, it has been proven that the substrate needs to show ionic bonding properties to affect growth through a graphene layer; furthermore, the potential field penetration depth increases with increased ionicity of substrate materials. As such, critical graphene thicknesses for remote epitaxy of GaAs (30% ionicity), GaN (50% ionicity) and LiF (90% ionicity) are 1 ML, 2 ML and 3 ML, respectively (Fig. 3c). Such finding has strong technical implications because most single-crystalline compound films can be grown on graphene on single-crystalline

substrates if graphene is sufficiently transparent to transmit atomic bonding potential of the substrate. Although progress has been done in the understanding of the mechanisms underlying this remote epitaxial effect, mastering of nucleation and growth are still required to obtain perfectly planar films with this method in the future.

Interplay between vdWE and remote epitaxy for 3D-on-2D. Since ionicity governs remote epitaxial field penetration through graphene, all compound materials could be grown via remote epitaxy as a perfect single-crystalline form. However, perfect transparency of remote interaction is not guaranteed in other 2D materials that have an ionic character as this can also play a role as an epitaxial seed layer³⁹. Some evidence that polarity of 2D materials affects nucleation and growth has been reported, with the orientation and nucleation density of 3D materials grown on hBN or MoS₂ being influenced by these materials^{27,40}.

This characteristic can be used to tune the epitaxial mode of 3D materials on polar 2D materials by varying the number of monolayers³⁹. For example, 1 ML hBN is not thick enough to screen the field from the GaN substrate, hence remote epitaxy can still occur. In fact, GaN grown on 1 ML hBN/GaN substrates shows two different azimuthal orientations; one follows the orientation of the hBN ML and the second is seeded to the GaN substrate (Fig. 3d). Thus, both vdWE and remote epitaxy occur simultaneously; in contrast, only vdWE occurs when 3 ML hBN interlayer is used, as the substrate potential field is completely screened (Fig. 3d). In the case of graphene, the substrate field is well transmitted through 1 ML owing to the non-polarity of this material; still, GaN films grown on 3 ML graphene is polycrystalline, this time due to insufficient seeding effect from the substrate. Some design rules for the realization of crystalline 3D-on-2D heterostructures can be inferred by this analysis. First, the thickness of 2D materials is crucial to determine

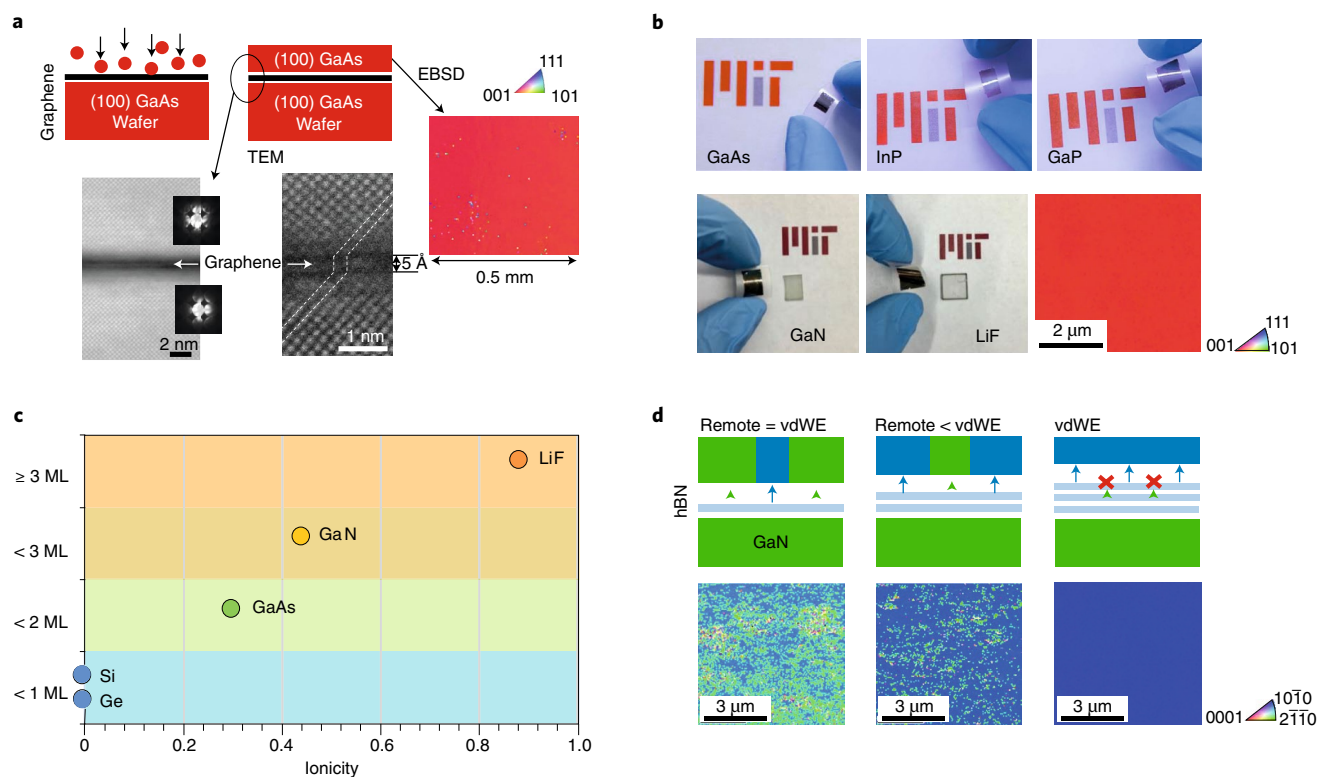


Fig. 3 | Remote epitaxy of various materials on 2D materials-coated substrates and interplay between remote epitaxy and vdWE. a, EBSD of remote epitaxial GaAs and cross-sectional TEM at GaAs/graphene/GaAs interface showing atomic interaction of GaAs through graphene. **b**, Photographs of freestanding films obtained by 2DLT after remote epitaxy including GaAs, InP, GaP, GaN and LiF, and representative EBSD taken on remote epitaxial films showing single-crystallinity of all compound remote epitaxial layers. **c**, The plot of rules of remote epitaxy that describes remote interaction penetration depth versus ionicity. **d**, Schematic (top) and EBSD (bottom) of the exfoliated surface of GaN on 1 ML hBN/GaN (left), 2 ML hBN/GaN (middle) and 3 ML hBN/GaN (right). Adapted from ref. ²⁵, SNL (**a,b**); and ref. ³⁹, SNL (**c,d**).

the growth mode (either vdWE or remote epitaxy). Thus, depositing thick 2D materials on the substrates must be ensured to secure the complete vdWE mode, whereas the thickness of 2D materials must be minimized to promote remote epitaxy. Second, polarity of 2D materials must be enhanced to promote vdWE whereas that of 3D materials must be strengthened to ensure remote epitaxy. It is important to mention that the epitaxy mode could be also influenced by the quality of the 2D materials and by the process used to deposit them on the 3D substrate. For example, polycrystalline graphene transferred by wet transfer did not show lattice transparency and produced a polycrystalline epilayer²⁵. This might be attributed to trapped molecules at the interface, which could disrupt atomic interactions through graphene; also, polycrystallinity of the 2D layer may induce non-uniformity in these atomic interactions.

3D/2D physical coupling and applications

Compared with pure vdW interaction between 2D materials, 3D/2D interactions such as ionic-vdW and covalent-vdW interactions can have more sophisticated coupling effects and produce unique physical properties. 2D materials do not present surface dangling bonds and hence require no hybridization of atomic orbital across the heterostructure interface, alleviating the issue of lattice mismatch that commonly limits monolithic heterointegration of 3D material-based heterostructures. The atom-thick 2D materials are almost transparent to externally applied energy such as electrical field, electromagnetic wave and chemical interaction. With such features, 3D/2D heterointegration offers the potential to achieve unprecedented device functions. In this section, we give an overview of unique 3D/2D coupling and relevant applications.

Electrical coupling. Ultrafast charge transfer (in the order of femtoseconds) between weak vdW interfaces—a topic of intense research due to its potential impact on electronics—has been seen not only between two 2D materials^{41–43}, but also between 2D and 3D materials⁴⁴. A recent demonstration showed that by constructing a heterostructure of single-crystalline Ge (110) grown on patches of monolayer MoS₂ (a top-view scanning electron microscopy (SEM) image in Fig. 4a, and a cross-sectional transmission electron microscopy (TEM) image in Fig. 4b⁴⁴), MoS₂ switches its doping type and the Ge becomes virtually doped, which is mainly caused by the charge transfer across the interface as revealed by density functional theory calculations. While the usual method of doping a semiconductor is to introduce dopant atoms during the crystal growth to provide extra electrons or holes, the doping in 2D materials can also be introduced by charge transfer from external sources, such as adjunct materials or acid/base^{45,46}. This can be applied to other 3D/2D heterostructure systems for doping modulation that cannot be achieved on 2D-on-2D or 3D-on-3D systems. Similarly, for the charge-density wave (CDW), phase transition was observed in tantalum disulfide (TaS₂) capped by hBN^{47,48}. The CDW phase transition in TaS₂ occurred at room temperature upon the charge modulation driven by graphene-based transistors, which implies that charge transfer in 3D/2D heterostructures could open a new design rule for CDW-based oscillators.

3D/2D electrical coupling can actually boost the device performance of heterostructures, with the barrier variable device (also called a barrister) being a typical example. One of the first demonstrations was achieved by creating an atomically sharp

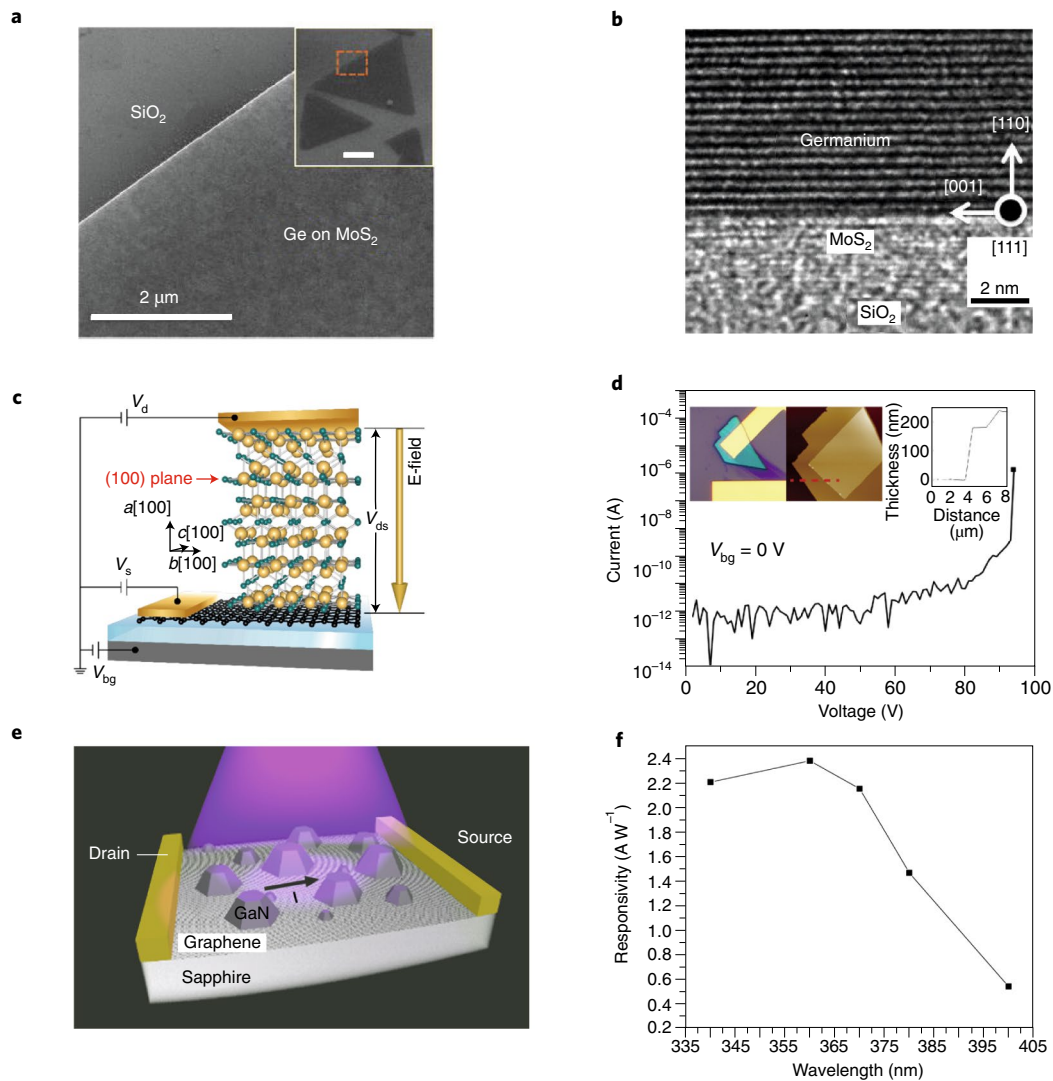


Fig. 4 | Electrically coupled 3D/2D devices. **a**, Top-view SEM of single-crystalline Ge grown on MoS₂ flake via low-pressure chemical vapour deposition. **b**, Cross-sectional TEM image of epitaxial Ge/MoS₂/SiO₂ interface. Charge transfer between Ge and MoS₂ results in highly conductive Ge and change of doping polarity of MoS₂ layer from n-type to p-type. **c**, Schematic diagram of a vertical Ga₂O₃/graphene power device, where the E-field is subject perpendicular to the (100) plane. **d**, Breakdown voltage of the graphene/Ga₂O₃ device shown in **c**. **e**, Schematic image of self-assembled GaN/graphene UV detector. **f**, Spectral responsivity of the GaN/graphene UV photodetector. Reproduced from ref. ⁴⁴, RSC (**a,b**); ref. ⁵⁰, AIP (**c,d**); and ref. ⁵¹, American Chemical Society (**e,f**).

interface between monolayer graphene and hydrogenated Si⁴⁹. A gate electrode modulates the electrostatic potential, thereby changing the Schottky barrier between the graphene and Si and controlling the charge transport across a three-terminal vertically stacked structure. A record on/off ratio of $\sim 10^5$ was demonstrated, which is on par with conventional complementary metal–oxide–semiconductor transistors and exceeds the requirements for robust logic operations. Moreover, it has scaling advantages over conventional transistors since the channel is formed vertically instead of laterally. Recently, gallium oxide (Ga₂O₃) has been gaining attention as a promising candidate for power electronics because of its high theoretical breakdown field of 8 MV cm⁻¹, but the lateral devices showed much lower performance (~ 4 MV cm⁻¹). By heterogeneously transferring Ga₂O₃ on top of a monolayer graphene on SiO₂/Si back gate, building a vertical structure, a breakdown field of nearly 5.2 MV cm⁻¹ was achieved (schematic of the device is shown in Fig. 4c and breakdown characteristics in Fig. 4d)⁵⁰, owing to the fact that the crystal orientation perpendicular to the (100) plane of Ga₂O₃ is more resistant to electrical

breakdown compared with the orientation parallel to the (100) plane. The β -Ga₂O₃/graphene device shows barrister-like gate-tunable I–V characteristics, with the electrons injected from graphene while the back gate can still penetrate the graphene and modulate the Ga₂O₃ channel.

More recently, enhanced photodetection performance has also been demonstrated by 3D/2D electrical coupling, in a hybrid III–N/2D ultraviolet (UV) photodetector realized by epitaxy of GaN on graphene/sapphire substrates (device schematic shown in Fig. 4e)⁵¹. In this structure, GaN–graphene interface has a built-in electric field and the GaN energy bands bends upwards, creating a barrier for electrons and a well into graphene for holes. When UV photons are absorbed by the GaN, the electrons are trapped in the GaN and the holes are drifted into graphene. This modulates the Fermi-level of the graphene, changing its conductivity, which can be probed using simple Ti/Au contacts. A high photoresponsivity of 2.5 A W⁻¹ was achieved for photons of wavelength 340–360 nm and power of 10 μW cm⁻² (Fig. 4f), while typical ZnO-based UV photodetectors have a responsivity in the range of ~ 1 A W⁻¹ (ref. ⁵²).

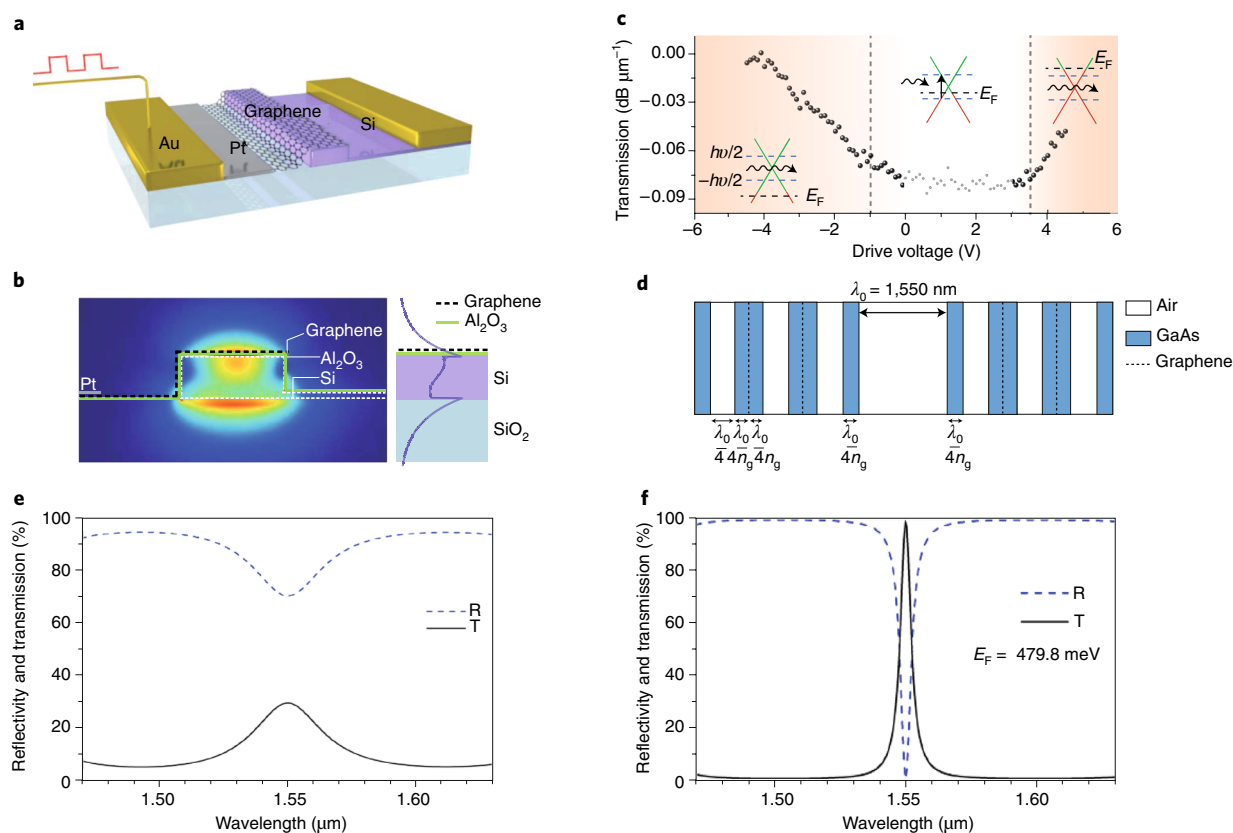


Fig. 5 | Optically coupled 3D/2D devices. **a**, Schematic of an electrically controlled gated graphene optical modulator on silicon waveguide. **b**, Cross-sectional view of waveguide shown in **a** with an overlay of the optical mode plot. The graphene is transferred onto a Si waveguide passivated by a thin Al₂O₃ layer. **c**, Transmission modulation of graphene as a function of drive voltage using a laser with wavelength of 1.53 μm. Three regions of modulation are observed. In the middle region, the Fermi level is near the Dirac point, allowing interband transitions. For left and right regions, the Fermi level is either below or above the Dirac point, preventing photon absorption and thereby increasing transmission. **d**, Schematic illustration of a GaAs/graphene/GaAs structure for high-efficiency transmission filter applications. **e**, Reflectivity and transmission of the stack shown in **d** without graphene embedded in the GaAs regions. **f**, Reflectivity and transmission of the stack shown in **d** when graphene Fermi level is at 479.8 meV. Reproduced from ref. ⁵³, SNL (**a-c**). Adapted from ref. ⁵⁹, Elsevier (**d-f**).

All-optical coupling. 3D/2D optical coupling can play a critical role in improving the performance over 3D or 2D standalone optoelectronic devices. Several works already show broadband and ultrafast optical tunability of graphene on insulating templates by controlling the charge density in graphene^{53–58}. An illustration and cross-sectional schematic of a broadband graphene optical modulator integrated with a silicon waveguide is shown in Fig. 5a,b. The modulation achieved using a 1.53-μm laser is shown in Fig. 5c. The modulation is a consequence of the Fermi-level shift with respect to the Dirac point. If the Fermi-level is near the Dirac point, interband transition is allowed and absorption is high. However, if the Fermi-level is sufficiently below or above the Dirac point, electrons are depleted or interband transition is forbidden, respectively, and thus absorption is low (as illustrated as insets to Fig. 5c). Despite the extraordinary optical tunability of graphene, a large gate bias of tens of volts was required for modulation, which is undesirable in practical settings⁵⁴. Sandwiching or inserting graphene inside a depletion region of a p–n junction may greatly reduce the voltage needed and improve the modulation speed as the process is assisted by drift instead of diffusion. Preliminary work on such a structure reported an order of magnitude lower voltage for modulating graphene transmittance up to 50% for 1.3-μm light, comparable to state-of-the-art electro-absorption modulators⁵⁸. A simple transmission matrix method simulation predicted that graphene–GaAs–graphene stacked layers could achieve nearly 100% transmission

filter at the most critical wavelength of 1.55 μm for optical communication (detailed structure design in Fig. 5d; simulated reflectivity and transmission in Fig. 5f)⁵⁹, while only about 30% transmission is possible without graphene in the structure (Fig. 5e)⁵⁹. Beyond graphene, it was noted that other 2D materials such as TMDs could be useful for optoelectronics combined with inorganic materials including Si and GaAs, because of their unique properties such as high carrier mobility, stability and flexibility^{19,20,60}.

Thermal coupling. Thermal management is a key issue in device performance and reliability for nearly all opto-electrical and electrical devices. Passive cooling at the package level and external active cooling, which are commonly used for thermal management, are often inefficient and may require extra power. Therefore, passive cooling at the device level is a crucial need for applications such as light-emitting diodes (LEDs), power devices and integrated circuits (IC) that all produce heat through joule heating. Conventional methods to reduce heating at the device level mainly use an alternative substrate with a higher thermal conductivity (such as expensive SiC substrates with thermal conductivity of 100–350 W m⁻¹ K⁻¹ instead of sapphire substrates with thermal conductivity of 30 W m⁻¹ K⁻¹). Single-layer graphene is known to have thermal conductivity in the range of 3,000–5,000 W m⁻¹ K⁻¹ (refs. ^{61–68}), which is much higher than the bulk graphite limit of 2,000 W m⁻¹ K⁻¹ and potentially higher than carbon nanotubes

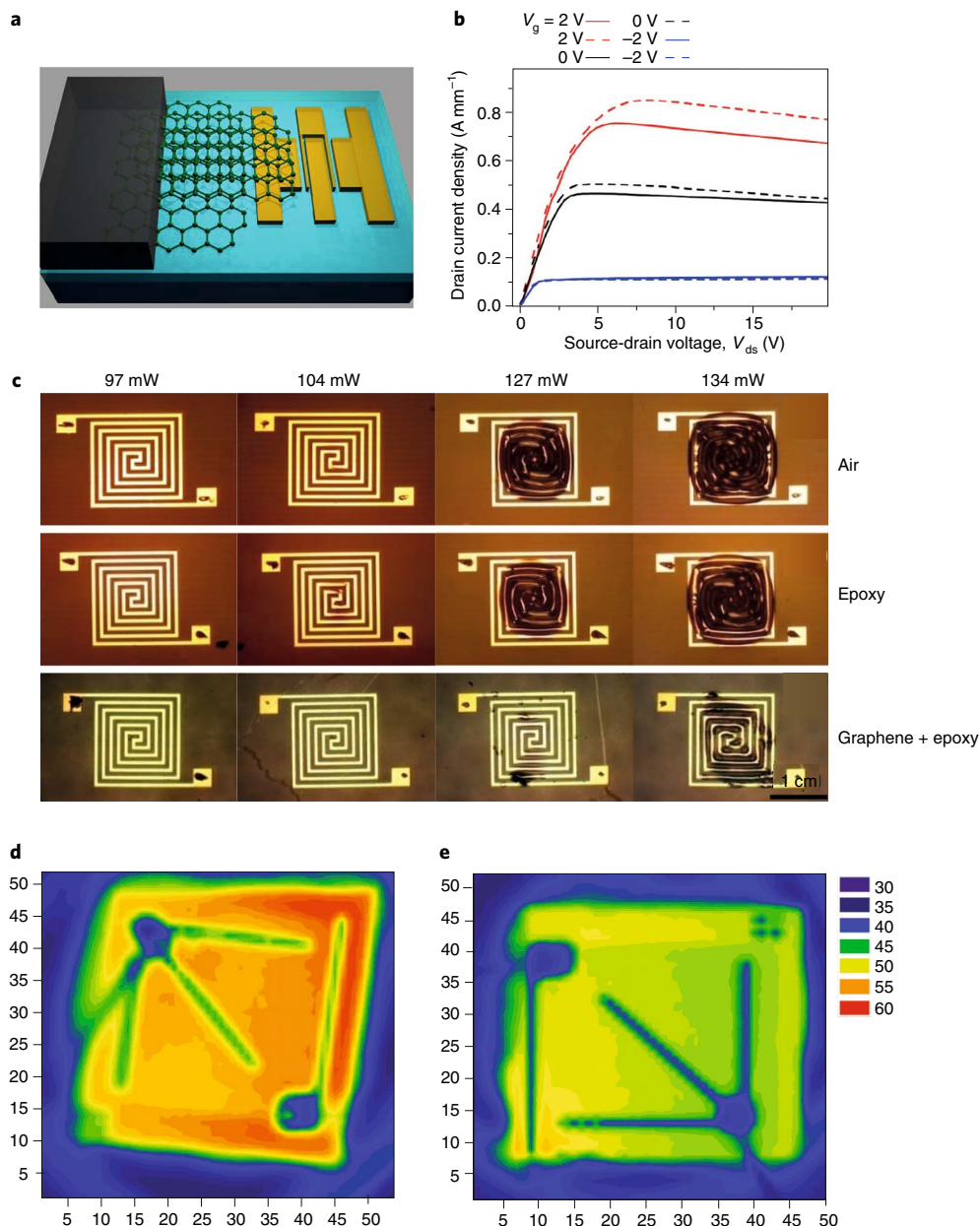


Fig. 6 | Heat coupling in 3D/2D structures. **a**, Schematic illustration of graphene heat spreader on a lateral transistor. **b**, Enhancement of drain current with (dotted lines) and without (solid lines) graphene heat sink. **c**, Serpentine heating element showing graphene as an efficient heat dissipater compared to air or epoxy. **d,e**, Temperature profile of InGaN/GaN LED without graphene oxide heat spreader (**d**) and with graphene oxide heat spreader (**e**). Reproduced from ref. ⁶⁶, SNL (**a,b**); ref. ⁶⁸, IEEE (**c**); and ref. ⁶⁷, SNL (**d,e**).

($2,000\text{ W m}^{-1}\text{ K}^{-1}$)⁶¹. Several groups have attempted to employ it as a device-level heat sink by transferring or growing graphene near the active area of the device. For example, graphene quilts have been demonstrated to reduce the operating temperature of AlGaIn/GaN high-electron-mobility transistors grown on sapphire by up to $70\text{ }^\circ\text{C}$, improving the drain current at high current densities (Fig. 6a,b)^{66,69}. A hot spot test was carried out to prove the heat spreading assisted by graphene (Fig. 6c). Similar phenomena were reported in graphene-based composites, where the graphene is utilized as thermal interface material for heat management in high-power-density communication devices^{70,71}. We note that TMDs and hBN have a relatively lower thermal conductivity in the hundreds of $\text{W m}^{-1}\text{ K}^{-1}$ compared with graphene, but are still better than conventional heat sinks.

The use of graphene oxide as a heat sink was demonstrated on InGaIn/GaN LEDs, where graphene oxide was deposited on a patterned sapphire substrate, leaving hole patterns open for lateral growth of an InGaIn/GaN LED structure (Fig. 6d)⁶⁷. The junction temperature, T_j , decreased by nearly 26% (Fig. 6e). Considering thermal droop is a serious issue for high power LEDs⁷², using graphene as a buffer between the InGaIn/GaN and sapphire to allow better heat spreading is a viable method for improving the device performance at low cost and with almost zero extra power requirement.

Lattice/strain decoupling. For inorganic devices epitaxially grown on the rigid substrate, strain is typically unavoidable owing to inherent lattice mismatch between different materials. Strained epitaxial device layers can degrade or even stop functioning due to cracking,

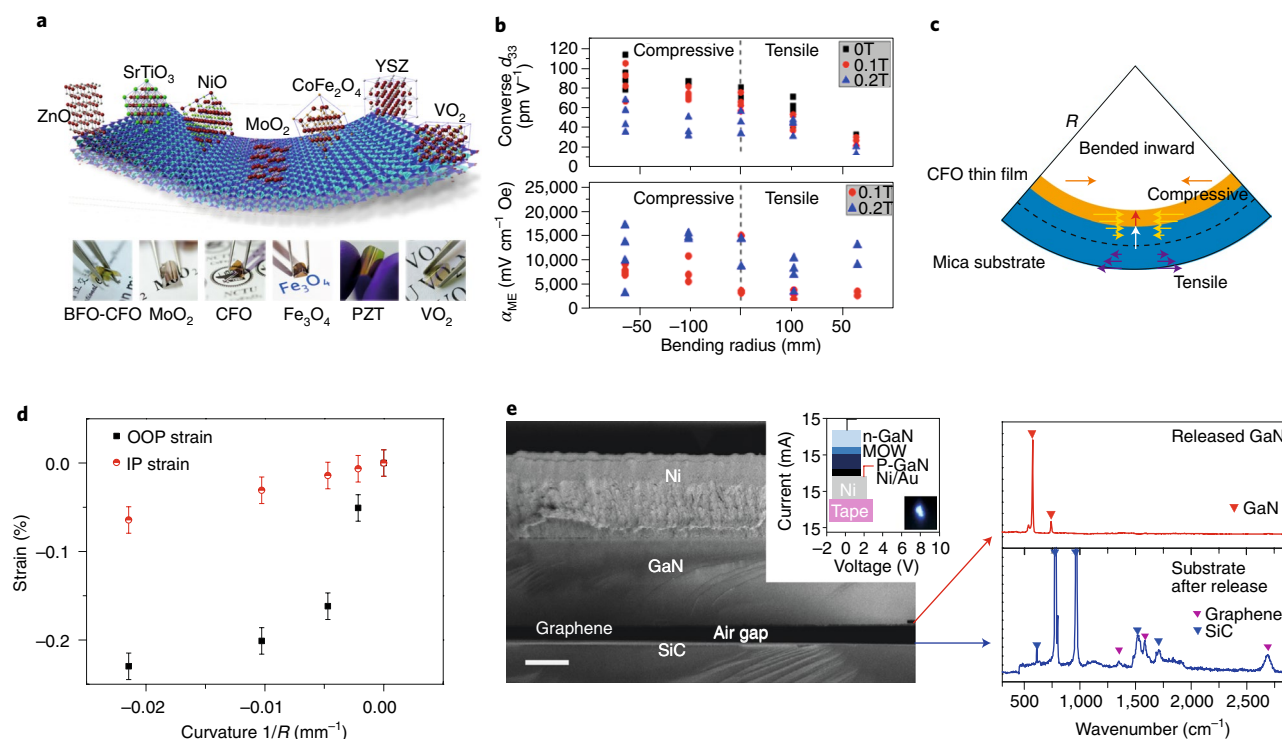


Fig. 7 | Lattice decoupling and vdW coupling in 3D/2D structures. **a**, Schematic illustration of vdW growth of various complex oxide materials on mica substrates. **b**, Change in d_{33} (pm V⁻¹) and magnetoelectric (α_{ME} mV cm⁻¹ Oe⁻¹) coupling characteristics of BFO-CFO nanocomposite as a function of bending radius of the mica substrate⁷⁷. **c**, Schematic illustration of bending radius and strain% of complex oxide CFO film grown on flexible mica. **d**, Negligible in-plane (IP) and out-of-plane (OOP) strain of the CFO film in the order of 0.2% for a curvature of 0.02 mm⁻¹. The film thickness for each oxide material presented here is much thinner than the mica substrate so that the in-plane strain is uniform across the entire oxide layer. **e**, SEM image of exfoliated GaN epilayers precisely from the surface of graphene on SiC by the Ni stressor. Blue LED light emission from exfoliated GaN/InGaN grown on reused epitaxial graphene/SiC substrate (inset data). Raman shows that graphene left on the SiC substrate after peeling. Reproduced from ref. ⁷⁸, SNA (**a**); and ref. ⁷⁵, American Chemical Society (**c,d**). Adapted from ref. ⁷⁶, American Chemical Society (**b**); and ref. ³⁸, SNL (**e**).

delamination or dislocating. In even higher mismatch conditions, epitaxial growths of device layers are not permitted. This strain coupling can be weakened for thin films grown on flexible vdW substrates, allowing extreme flexibility without adversely affecting their physical characteristics. Taking oxide materials, for example (illustrated in Fig. 7a⁷³⁻⁷⁹), vdWE can successfully suppress the strain in the grown films so that their unique properties, such as ferroelectric, ferromagnetic and multiferroic properties, can be preserved. For instances, BiFeO₃ (BFO)-CoFe₂O₄ (CFO) nanocomposites grown on mica exhibited extremely small change in piezoelectric coefficient d_{33} (pm V⁻¹) and magnetoelectric coupling coefficient (α_{ME} mV cm⁻¹ Oe⁻¹) with low bending radius of the mica substrate⁷⁵ (Fig. 7b). Similarly, for VO₂, negligible change in its resistance was observed with a bending radius as low as 5 mm (ref. ⁷⁷). The CFO film grown on mica only showed a maximum of 0.2% strain at a curvature of -0.02 mm⁻¹ (Fig. 7c,d). All films presented no signs of degradation after nearly 10⁵ cycles of bending, due to the weak strain coupling between the film and the substrate⁷⁴.

Van der Waals coupling. Various wafer-recycling techniques such as chemical lift-off⁸⁰, optical lift-off⁸¹ and mechanical lift-off⁸² have been developed in the past few decades. However, none of the existing methods can offer following advantages simultaneously for significantly reducing manufacturing costs: (1) substrate reusability, (2) a minimal substrate-refurbishment step after the layer release, (3) a fast release rate, and (4) precise control of release thickness. 2D materials-based layer transfer (2DLT) process has shown great potential to meet all the above requirements. Once the perfect single-crystalline 3D materials are grown on 2D materials via vdWE

or remote epitaxy, the epilayers can be released from the 3D/2D interface by mechanical exfoliation due to their extremely weak vdW coupling. Crack propagation can be precisely guided along the interface such that underlying substrates may not be damaged during the separation process^{23,24,37}. The substrate can be potentially reused infinitely, saving the cost of semiconductor processing. The ultrafast mechanical exfoliation of entire 3D films (a few seconds) can also increase throughput of manufacturing processes.

The 2DLT process has been first demonstrated in III-N material systems. Wafer-scale GaN/InGaN LEDs were grown on hBN via vdWE and entire LED stacks were completely exfoliated from hBN³¹. Later, high-electron-mobility transistors were grown on hBN and transferred onto Cu substrates for effective heat dissipation⁸³. Exfoliated GaN/InGaN structures, which were grown on reused epitaxial graphene/SiC substrates, exhibit blue light emission³⁸ (Fig. 7e). The 2DLT process, which can produce freestanding single-crystalline films, will offer great flexibility to design 3D/3D, 3D/2D, 2D/3D mixed heterostructures for overcoming fundamental challenges in conventional 3D heterostructures, and opens up new opportunity for next-generation flexible electronics that currently have been limited by the selection of flexible functional materials.

Perspective

All modern innovations in electronics had been based on 3D material systems until the advent of graphene, the first 2D material, discovered in 2004. 2D materials in heterostructures can be designed to operate as an active element or as an interfacial element, enabling new architectures in which 3D and 2D materials are physically coupled to each other. In this section, we will discuss future research

directions of 3D/2D heterointegrated structures and remaining challenges.

Charge transfer from 2D materials to 3D semiconductors via electrical coupling, modulating their doping states, permit great flexibility in designing semiconductor heterojunctions⁴⁵. Such electrical 3D/2D coupling can enhance doping of semiconductors beyond its limit because of solid solubility of dopants. For example, it may unlock the way to enhance the p-type doping in GaN, which has been a persistent issue for more than a decade⁸⁴, by appropriate selection of coupling materials. Recent discovery of electrically tunable superconductivity in a topological insulator, such as tungsten ditelluride (WTe₂) with topological phase changing to superconducting under electrical stimuli⁸⁵, suggests another interesting direction. Electrical coupling could offer a platform combining superconducting and topological phases of matter and forming superconducting junctions. Another direction is the modulation of the spin-orbit interaction in 2D materials by the electrical 3D/2D coupling as quantum anomalous Hall effect in standalone 2D materials has been observed under applied electrical field⁸⁶.

While most demonstrations of 3D/2D optical coupling have been done on graphene/conventional bulk materials, integration of TMDs with bulk semiconductors promises great potential to enhance this coupling as the refractive index of monolayer TMDs can be largely modulated via an applied electric field⁸⁷. It was reported that the imaginary and real part of the refractive index of MoS₂, WSe₂ and WS₂ can be tuned by >60% and >20%, respectively, under electrical bias. Thus, 3D/2D integration opens the opportunity to design a new functional architecture for advanced optoelectronic applications.

Strain decoupling at 3D/2D interface has great potential to enhance the performance of complex functional oxides by eliminating the substrate clamping effect, an inherent bottleneck in the field. Remote homoepitaxy of complex oxides and subsequent lift-off of the grown films via weak vdW coupling at the interface can produce freestanding single-crystalline oxides. Such films can be substantially strained to achieve a larger freedom of tuning their physical properties, while in conventional pseudomorphic epitaxy it is limited by the critical thickness of generating defects due to strain energy accumulation. Also, such released functional oxide films can be stacked together for potential magnetoelectric coupling applications⁸⁸.

Successful single-crystalline 3D materials grown on 2D materials, along with rapid mechanical release and transfer of device structures, will potentially revolutionize current electronics, optics and photonics industries. Remote homoepitaxy of GaN on free-standing GaN wafers without dislocations can uniquely offer a solution for low-cost fabrication of high-performance III-N lasers or vertical III-N devices. More excitingly, released ultrathin films can be hetero-integrated onto flexible substrates^{89,90}, providing an opportunity for inorganic-based flexible electronics outperforming organic ones.

Besides 3D/2D heterostructures discussed so far, there are many interesting topics to explore in 3D/2D/3D multi-heterostructures. For example, 3D/2D/3D systems with a well-defined periodicity can have two moiré patterns in both heterointerfaces, which can be tuned via rotation-controllable film transfer techniques⁹¹. Novel physics has emerged by intentional crystallographic misorientation of crystal lattices in 2D/2D systems^{91–95}, such as unconventional superconductivity arising from a twisted graphene superlattice in its ‘magic angle’^{92,93}. At the heterointerfaces, localized phonon–electron coupling may present an opportunity of manipulating optical and electrical properties in 3D/2D/3D systems.

Precise transfer technique of 2D materials together with single-crystalline growth of 3D materials on 2D materials can offer a great opportunity to fabricate 3D/2D/3D heterostructured systems and discover new physics. 2D materials intercalated between 3D

material quantum well structures may actively interact with a two-dimensional electron gas (2DEG)^{96–99}, and thus provide high Fermi velocity (v_F) caused by substantial doping, superior to that achieved by external field control¹⁰⁰. 3D/2D/3D heterostructures may also facilitate localized carriers in atomically thin 2D materials, forming many-body systems such as biexciton and trion, similar to the enhanced photoluminescence due to large electron–hole overlap in trilayer 2D heterostructures¹⁰¹.

To form various 3D/2D heterostructures proposed above, maintaining pristine interfaces is crucial via ultraclean transfer or direct growth techniques. Up until now, there has been a trade-off between obtaining clean interface and achieving large-size samples. Wafer-scale transfer and heterointegration of monolayer 2D materials have been recently demonstrated, taking advantage of interfacial toughness contrast, which showed the possibility of fabricating 2D material devices on a large scale¹⁰². However, some challenges still remain for fully integrating 2D materials into commercial opto-electrical and electrical devices. For example, although the dry-transfer technique using metal films (for example, Ni, Au or Cu) avoid polymer residues, nanoscale metal particles may remain, potentially reducing device reliability and accelerating degradation due to metal particle migration (causing leakage paths or shorting) when integrated with conventional bulk devices. A transfer method without using any sort of metal or polymer adhesive layer is desirable. Another important aspect that needs to be developed is robust detection of nanoscale defects and impurities such as tears, holes and wrinkles of 2D materials at wafer scale. New or existing methods can be used—for example, confocal laser scanning was recently reported to non-destructively probe macroscopic defects of graphene films with a quick turnaround time. Additionally, a comprehensive understanding of device performance with respect to defects in 2D materials has yet to be explored. Identifying key defects and how they affect device performance, as well as a quick robust method of detecting such defects, will become increasingly important.

In this Review, we have presented a comprehensive overview of methods for forming 3D/2D heterostructures, their applications for next-generation integrated systems via physical coupling, and remaining challenges in fabrication. Integrating 3D and 2D materials widens the spectrum of building blocks for creating hybrid systems with unique functionalities and excellent performance. This will give a high degree of design and manufacturing freedom to research communities and industries.

Received: 19 October 2018; Accepted: 6 March 2019;
Published online: 21 May 2019

References

- Ruzmetov, D. et al. Vertical 2D/3D semiconductor heterostructures based on epitaxial molybdenum disulfide and gallium nitride. *ACS Nano* **10**, 3580–3588 (2016).
- Zhang, Q., Fiori, G. & Iannaccone, G. On transport in vertical graphene heterostructures. *IEEE Electron Device Lett.* **35**, 966–968 (2014).
- Huang, B., Xiang, H., Yu, J. & Wei, S. Effective control of the charge and magnetic states of transition-metal atoms on single-layer boron nitride. *Phys. Rev. Lett.* **108**, 206802 (2012).
- Konstantatos, G. et al. Hybrid graphene–quantum dot phototransistors with ultrahigh gain. *Nat. Nanotechnol.* **7**, 363–368 (2012).
- Al Balushi, Z. Y. et al. Two-dimensional gallium nitride realized via graphene encapsulation. *Nat. Mater.* **15**, 1166–1171 (2016).
- Journot, T., Bouchiat, V., Gayral, B., Dijon, J. & Hyot, B. Self-assembled UV photodetector made by direct epitaxial GaN growth on graphene. *ACS Appl. Mater. Interfaces* **10**, 18857–18862 (2018).
- Koma, A., Sunouchi, K. & Miyajima, T. Fabrication of ultrathin heterostructures with van der Waals epitaxy. *J. Vac. Sci. Technol. B* **3**, 724 (1985).
- Koma, A., Sunouchi, K. & Miyajima, T. Fabrication and characterization of heterostructures with subnanometer thickness. *Microelectron. Eng.* **2**, 129–136 (1984).
- van der Zande, A. M. et al. Grains and grain boundaries in highly crystalline monolayer molybdenum disulfide. *Nat. Mater.* **12**, 554–561 (2013).

10. Tsen, A. W. et al. Tailoring electrical transport across grain boundaries in polycrystalline graphene. *Science* **336**, 1143–1146 (2012).
11. Zhang, Y. et al. Direct observation of the transition from indirect to direct bandgap in atomically thin epitaxial MoSe₂. *Nat. Nanotechnol.* **9**, 111–115 (2014).
12. Zhang, Y. et al. Thickness considerations of two-dimensional layered semiconductors for transistor applications. *Sci. Rep.* **6**, 29615 (2016).
13. Kang, K. et al. High-mobility three-atom-thick semiconducting films with wafer-scale homogeneity. *Nature* **520**, 656–660 (2015).
14. Emtsev, K. V. et al. Towards wafer-size graphene layers by atmospheric pressure graphitization of silicon carbide. *Nat. Mater.* **8**, 203–207 (2009).
15. Lee, J. et al. Wafer-scale growth of single-crystal monolayer graphene on reusable hydrogen-terminated germanium. *Science* **344**, 286–290 (2014).
16. Novoselov, K. S. et al. Electric field effect in atomically thin carbon films. *Science* **306**, 666–669 (2004).
17. Li, X. et al. Transfer of large-area graphene films for high-performance transparent conductive electrodes. *Nano Lett.* **9**, 4359–4363 (2009).
18. Kim, K. S. et al. Large-scale pattern growth of graphene films for stretchable transparent electrodes. *Nature* **457**, 706–710 (2009).
19. Yim, C. et al. Heterojunction hybrid devices from vapor phase grown MoS₂. *Sci. Rep.* **4**, 5458 (2014).
20. Yim, C. et al. High-performance hybrid electronic devices from layered PtSe₂ films grown at low temperature. *ACS Nano* **10**, 9550–9558 (2016).
21. Lupina, G. et al. Residual metallic contamination of transferred chemical vapor deposited graphene. *ACS Nano* **9**, 4776–4785 (2015).
22. Bae, S.-H. et al. Unveiling the carrier transport mechanism in epitaxial graphene for forming wafer-scale, single-domain graphene. *Proc. Natl Acad. Sci.* **114**, 4082–4086 (2017).
23. Kim, J. et al. Layer-resolved graphene transfer via engineered strain layers. *Science* **342**, 833–836 (2013).
24. Desai, S. B. et al. Gold-mediated exfoliation of ultralarge optoelectronically-perfect monolayers. *Adv. Mater.* **28**, 4053–4058 (2016).
25. Kim, Y. et al. Remote epitaxy through graphene enables two-dimensional material-based layer transfer. *Nature* **544**, 340–343 (2017).
26. Chung, K., Lee, C. H. & Yi, G. C. Transferable GaN layers grown on ZnO-coated graphene layers for optoelectronic devices. *Science* **330**, 655–657 (2010).
27. Kobayashi, Y., Kumakura, K., Akasaka, T. & Makimoto, T. Layered boron nitride as a release layer for mechanical transfer of GaN-based devices. *Nature* **484**, 223–227 (2012).
28. Hong, Y. J., Lee, W. H., Wu, Y., Ruoff, R. S. & Fukui, T. van der Waals epitaxy of InAs nanowires vertically aligned on single-layer graphene. *Nano Lett.* **12**, 1431–1436 (2012).
29. Gupta, P. et al. MOVPE growth of semipolar III-nitride semiconductors on CVD graphene. *J. Cryst. Growth* **372**, 105–108 (2013).
30. Chae, S. J. et al. Direct growth of etch pit-free GaN crystals on few-layer graphene. *RSC Adv.* **5**, 1343–1349 (2015).
31. Ayari, T. et al. Wafer-scale controlled exfoliation of metal organic vapor phase epitaxy grown InGaN/GaN multi quantum well structures using low-tack two-dimensional layered hBN. *Appl. Phys. Lett.* **108**, 171106 (2016).
32. Utama, M. I. B. et al. Incommensurate van der Waals epitaxy of nanowire arrays: a case study with ZnO on muscovite mica substrates. *Nano Lett.* **12**, 2146–2152 (2012).
33. Alaskar, Y. et al. Theoretical and experimental study of highly textured GaAs on silicon using a graphene buffer layer. *J. Cryst. Growth* **425**, 268–273 (2015).
34. Mohseni, P. K. et al. Monolithic III-V nanowire solar cells on graphene via direct van der Waals epitaxy. *Adv. Mater.* **26**, 3755–3760 (2014).
35. Munshi, A. M. et al. Vertically aligned GaAs nanowires on graphite and few-layer graphene: generic model and epitaxial growth. *Nano Lett.* **12**, 4570–4576 (2012).
36. Yoo, H., Chung, K., In Park, S., Kim, M. & Yi, G.-C. Microstructural defects in GaN thin films grown on chemically vapor-deposited graphene layers. *Appl. Phys. Lett.* **102**, 051908 (2013).
37. Lee, J. Lattice transparency of graphene. *Nano Lett.* **17**, 1711–1718 (2017).
38. Kim, J. et al. Principle of direct van der Waals epitaxy of single-crystalline films on epitaxial graphene. *Nat. Commun.* **5**, 4836 (2014).
39. Kong, W. et al. Polarity governs atomic interaction through two-dimensional materials. *Nat. Mater.* **17**, 999–1004 (2018).
40. Ago, H. et al. Controlled van der Waals epitaxy of monolayer MoS₂ triangular domains on graphene. *ACS Appl. Mater. Interfaces* **7**, 5265–5273 (2015).
41. Hong, X. et al. Ultrafast charge transfer in atomically thin MoS₂/WS₂ heterostructures. *Nat. Nanotechnol.* **9**, 682–686 (2014).
42. Ceballos, F., Bellus, M. Z., Chiu, H. Y. & Zhao, H. Ultrafast charge separation and indirect exciton formation in a MoS₂-MoSe₂ van der Waals heterostructure. *ACS Nano* **8**, 12717–12724 (2014).
43. Yu, Y. et al. Equally efficient interlayer exciton relaxation and improved absorption in epitaxial and nonepitaxial MoS₂/WS₂ Heterostructures. *Nano Lett.* **15**, 486–491 (2015).
44. Lin, Y.-C. et al. Charge transfer in crystalline germanium/monolayer MoS₂ heterostructures prepared by chemical vapor deposition. *Nanoscale* **8**, 18675–18681 (2016).
45. Bae, S.-H. et al. Graphene-P (VDF-TrFE) multilayer film for flexible applications. *ACS Nano* **7**, 3130–3138 (2013).
46. Kwon, S.-J. et al. Extremely stable graphene electrodes doped with macromolecular acid. *Nat. Commun.* **9**, 2037 (2018).
47. Liu, G. et al. A charge-density-wave oscillator based on an integrated tantalum disulfide-boron nitride-graphene device operating at room temperature. *Nat. Nanotechnol.* **11**, 845–850 (2016).
48. Samnakay, R. et al. Zone-folded phonons and the commensurate-incommensurate charge-density-wave transition in 1T-TaSe₂ thin films. *Nano Lett.* **15**, 2965–2973 (2015).
49. Yang, H. et al. Graphene barristor, a triode device with a gate-controlled Schottky barrier. *Science* **336**, 1140–1144 (2012).
50. Yan, X., Esqueda, I. S., Ma, J., Tice, J. & Wang, H. High breakdown electric field in β-Ga₂O₃/graphene vertical barristor heterostructure. *Appl. Phys. Lett.* **112**, 032101 (2018).
51. Journot, T., Bouchiat, V., Gayral, B., Dijon, J. & Hyot, B. Self-assembled UV photodetector made by direct epitaxial GaN growth on graphene. *ACS Appl. Mater. Interfaces* **10**, 18857–18862 (2018).
52. Liang, S. et al. ZnO Schottky ultraviolet photodetectors. *J. Cryst. Growth* **225**, 110–113 (2001).
53. Liu, M. et al. A graphene-based broadband optical modulator. *Nature* **474**, 64–67 (2011).
54. Wang, F. et al. Gate variable optical transitions in graphene. *Science* **320**, 206–209 (2008).
55. Yao, B. et al. Gate-tunable frequency combs in graphene-nitride microresonators. *Nature* **558**, 410–414 (2018).
56. Yao, B. et al. Broadband gate-tunable terahertz plasmons in graphene heterostructures. *Nat. Photon.* **12**, 22–28 (2018).
57. Liu, M., Yin, X. & Zhang, X. Double-layer graphene optical modulator. *Nano Lett.* **12**, 1482–1485 (2012).
58. Yao, R. et al. Graphene/III-V hybrid diode optical modulator. In *Conf. Lasers Electro-Optics JTu2A.7* (2018).
59. Ajlani, H., Azizi, M. K., Gharsallah, A. & Oueslati, M. Graphene-GaAs-graphene stacked layers for the improvement of the transmission at the wavelength of 1.55 μm. *Opt. Mater.* **57**, 120–124 (2016).
60. Zeng, L. H. et al. Fast, self-driven, air-stable, and broadband photodetector based on vertically aligned PtSe₂/GaAs heterojunction. *Adv. Funct. Mater.* **28**, 1705970 (2018).
61. Balandin, A. A. et al. Superior thermal conductivity of single-layer graphene. *Nano Lett.* **8**, 902–907 (2008).
62. Subrina, S., Kotchetkov, D. & Balandin, A. A. Heat removal in silicon-on-insulator integrated circuits with graphene lateral heat spreaders. *IEEE Electron Device Lett.* **30**, 1281–1283 (2009).
63. Yan, R. et al. Thermal conductivity of monolayer molybdenum disulfide obtained from temperature-dependent Raman spectroscopy. *ACS Nano* **8**, 986–993 (2014).
64. Ahn, C. et al. Energy-efficient phase-change memory with graphene as a thermal barrier. *Nano Lett.* **15**, 6809–6814 (2015).
65. Balandin, A. A. Thermal properties of graphene and nanostructured carbon materials. *Nat. Mater.* **10**, 569–581 (2011).
66. Yan, Z., Liu, G., Khan, J. M. & Balandin, A. A. Graphene quilts for thermal management of high-power GaN transistors. *Nat. Commun.* **3**, 827 (2012).
67. Han, N. et al. Improved heat dissipation in gallium nitride light-emitting diodes with embedded graphene oxide pattern. *Nat. Commun.* **4**, 1452 (2013).
68. Bae, S.-H. et al. Graphene-based heat spreader for flexible electronic devices. *IEEE Trans. Electron Devices* **61**, 4171–4175 (2014).
69. Renteria, J., Nika, D. & Balandin, A. Graphene thermal properties: applications in thermal management and energy storage. *Appl. Sci.* **4**, 525–547 (2014).
70. Shahil, K. M. F. & Balandin, A. A. Graphene-multilayer graphene nanocomposites as highly efficient thermal interface materials. *Nano Lett.* **12**, 861–867 (2012).
71. Kargar, F. et al. Thermal percolation threshold and thermal properties of composites with high loading of graphene and boron nitride fillers. *ACS Appl. Mater. Interfaces* **10**, 37555–37565 (2018).
72. De Santi, C. et al. Role of defects in the thermal droop of InGaN-based light emitting diodes. *J. Appl. Phys.* **119**, 094501 (2016).
73. Bitla, Y. et al. Oxide heteroepitaxy for flexible optoelectronics. *ACS Appl. Mater. Interfaces* **8**, 32401–32407 (2016).
74. Jiang, J. et al. Flexible ferroelectric element based on van der Waals heteroepitaxy. *Sci. Adv.* **3**, e1700121 (2017).

75. Liu, H. J. et al. Flexible heteroepitaxy of CoFe_2O_4 /muscovite biphase with large magnetostriction. *ACS Appl. Mater. Interfaces* **9**, 7297–7304 (2017).
76. Amrillah, T. et al. Flexible multiferroic bulk heterojunction with giant magnetoelectric coupling via van der Waals epitaxy. *ACS Nano* **11**, 6122–6130 (2017).
77. Li, C.-I. et al. van der Waal epitaxy of flexible and transparent VO_2 film on muscovite. *Chem. Mater.* **28**, 3914–3919 (2016).
78. Chu, Y.-H. Van der Waals oxide heteroepitaxy. *npj Quantum Mater.* **2**, 67 (2017).
79. Lee, S. A., Hwang, J.-Y., Kim, E. S., Kim, S. W. & Choi, W. S. Highly oriented SrTiO_3 thin film on graphene substrate. *ACS Appl. Mater. Interfaces* **9**, 3246–3250 (2017).
80. Lee, K., Zimmerman, J. D., Xiao, X., Sun, K. & Forrest, S. R. Reuse of GaAs substrates for epitaxial lift-off by employing protection layers. *J. Appl. Phys.* **111**, 033527 (2012).
81. Iida, D. et al. Laser lift-off technique for freestanding GaN substrate using an in droplet formed by thermal decomposition of GaInN and its application to light-emitting diodes. *Appl. Phys. Lett.* **105**, 072101 (2014).
82. Bedell, S. W. et al. Layer transfer by controlled spalling. *J. Phys. D: Appl. Phys.* **46**, 152002 (2013).
83. Hiroki, M. et al. Suppression of self-heating effect in AlGaIn/GaN high electron mobility transistors by substrate-transfer technology using hBN. *Appl. Phys. Lett.* **105**, 193509 (2014).
84. Bernardini, F., Fiorentini, V. & Bosin, A. Theoretical evidence for efficient p-type doping of GaN using beryllium. *Appl. Phys. Lett.* **70**, 2990–2992 (1997).
85. Fatemi, V. et al. Electrically tunable low-density superconductivity in a monolayer topological insulator. *Science* **362**, 926–929 (2018).
86. Ezawa, M. Valley-polarized metals and quantum anomalous hall effect in silicene. *Phys. Rev. Lett.* **109**, 055502 (2012).
87. Yu, Y. et al. Giant gating tunability of optical refractive index in transition metal dichalcogenide monolayers. *Nano Lett.* **17**, 3613–3618 (2017).
88. Griggio, F. et al. Substrate clamping effects on irreversible domain wall dynamics in lead zirconate titanate thin films. *Phys. Rev. Lett.* **108**, 157604 (2012).
89. Park, S., Vosguerichian, M. & Bao, Z. A review of fabrication and applications of carbon nanotube film-based flexible electronics. *Nanoscale* **5**, 1727–1752 (2013).
90. Sun, Y. & Rogers, J. A. Inorganic semiconductors for flexible electronics. *Adv. Mater.* **19**, 1897–1916 (2007).
91. Ribeiro-Palau, R. et al. Twistable electronics with dynamically rotatable heterostructures. *Science* **361**, 690–693 (2018).
92. Cao, Y. et al. Unconventional superconductivity in magic-angle graphene superlattices. *Nature* **556**, 43–50 (2018).
93. Cao, Y. et al. Correlated insulator behaviour at half-filling in magic-angle graphene superlattices. *Nature* **556**, 80–84 (2018).
94. Chari, T., Ribeiro-Palau, R., Dean, C. R. & Shepard, K. Resistivity of rotated graphite-graphene contacts. *Nano Lett.* **16**, 4477–4482 (2016).
95. Moon, P., Son, Y. W. & Koshino, M. Optical absorption of twisted bilayer graphene with interlayer potential asymmetry. *Phys. Rev. B* **90**, 155427 (2014).
96. Hwang, H. Y. et al. Emergent phenomena at oxide interfaces. *Nat. Mater.* **11**, 103–113 (2012).
97. Novoselov, K. S. et al. Two-dimensional gas of massless Dirac fermions in graphene. *Nature* **438**, 197–200 (2005).
98. Sonde, S. et al. Role of graphene/substrate interface on the local transport properties of the two-dimensional electron gas. *Appl. Phys. Lett.* **97**, 132101 (2010).
99. Gibertini, M. et al. Engineering artificial graphene in a two-dimensional electron gas. *Phys. Rev. B* **79**, 241406 (2009).
100. Hwang, C. et al. Fermi velocity engineering in graphene by substrate modification. *Sci. Rep.* **2**, 590 (2012).
101. Choi, C. et al. Enhanced interlayer neutral excitons and trions in trilayer van der Waals heterostructures. *npj 2D Mater. Appl.* **2**, 30 (2018).
102. Shim, J. et al. Controlled crack propagation for atomic precision handling of wafer-scale two-dimensional materials. *Science* **362**, 665–670 (2018).

Competing interests

The authors declare no competing interests.

Additional information

Reprints and permissions information is available at www.nature.com/reprints.

Correspondence should be addressed to J.K.

Publisher's note: Springer Nature remains neutral with regard to jurisdictional claims in published maps and institutional affiliations.

© Springer Nature Limited 2019